Journal of Applied Polymer Science

Mass Production of Carbon Nanotube-Reinforced Polyacrylonitrile Fine Composite Fibers

Baicheng Weng, Fenghua Xu, Karen Lozano
Mechanical Engineering Department, The University of Texas—Pan American, Edinburg, Texas 78539
Correspondence to: K. Lozano (E-mail: lozanok@utpa.edu)

ABSTRACT: A facile and large-scale production method of polyacrylonitrile (PAN) fibers and carboxyl functionalized carbon nanotube reinforced PAN composite fibers was demonstrated by the use of Forcespinning® technology. The developed polymeric fibers and carbon nanotube-reinforced composite fibers were subsequently carbonized to obtain carbon fiber systems. Analysis of the fiber diameter, homogeneity, alignment of carbon nanotube and bead formation was conducted with scanning electron microscopy. Thermogravimetric analysis, electrical, and mechanical characterization were also conducted. Raman and FTIR analyses of the developed fiber systems indicate interactions between carbon nanotubes and the carbonized PAN fibers through π–π stacking. The carbonized carbon nanotube-reinforced PAN composite fibers possess promising applications in energy storage applications. © 2014 Wiley Periodicals, Inc. J. Appl. Polym. Sci. **2014**, *131*, 40302.

KEYWORDS: nanotubes; graphene and fullerenes; composites; fibers

Received 1 October 2013; accepted 14 December 2013
DOI: 10.1002/app.40302

INTRODUCTION

Since Roger Bacon demonstrated the formation of flexible and tough graphite in 1960,[1] the large scale production of these fibers by carbonization of polyacrylonitrile (PAN), rayon, or other polymers (e.g., pitch) has been extensively researched[2] to meet increasing needs to manufacture advanced composites. These fibers are the key component of structural composites.[3] The combination of fibers and matrices often gives rise to high strength materials with minimum weight. Therefore, carbon fiber-reinforced composites have been extensively used in a wide array of applications such as aircraft brakes, space structures, military and commercial planes, lithium batteries, sporting goods, and structural reinforcement in construction. However, after the discovery of carbon nanotube by Iijima in 1991,[4] researchers have placed a strong focus on the field of carbon nanotubes (CNTs)-reinforced materials. It is believed that the nanotube could be an ideal reinforcement in composites because of its excellent mechanical properties and electrical and thermal conductivity.[2]

A number of investigations have been carried out using CNTs as reinforcement in different matrices, namely polymer, ceramic, and metals.[5–13] For instance, the incorporation of CNTs into ceramic matrices leads to the enhancement in toughness and strength as well as in the electrical conductivity and thermal conductivity. Several recent studies report the inclusion of CNTs in ceramic materials, such as Al_2O_3, ZrO_2, SiC, and SiO_2-based glasses and glass ceramics. Chou and coworkers[13] developed CNT-silicon-carbide (SiC)/ceramic composites and reported a 10% improvement in the strength and fracture toughness when compared with the monolithic ceramics. Li et al.[14] found that the yield strength and ultimate tensile strength of carbon nanotube-reinforced Ti metal matrix composites are 40.4% and 11.4% higher than the Ti metal. For hard matrix composites, the fracture toughness can be improved effectively by increasing the CNT length. The most intensively studied composites are CNT-reinforced polymers. The modulus and tensile strength have been reported to improve from several percent up to more than 100 percent, depending on the polymer matrix, concentration of CNTs, and type of CNT. CNT-reinforced polymer fibers have also been recently studied, e.g., Dror et al.[15] reported electrospun polyethylene oxide fibers containing low concentrations of multiwalled CNTs. Ko et al.[16] also reported continuous CNT filled fiber yarns made by electrospinning. They found the modulus was improved 120% in fibers containing 4 wt % of single-walled CNT (SWCNT) within the fibers.

Studies related to CNT-reinforced fibers with improved mechanical, thermal, and electrical properties and increased surface area are highly demanded, due to increasing requirements of space and energy storage materials, in which carbon fibers (CFs) are intensively used. For instance, nose tip and wing tip of space shuttles have to endure temperatures higher than 2760°C. For the above-mentioned applications, carbon composite fibers

should be further improved for high-temperature endurance, high strength, high thermal conductivity, high fatigue resistance, and light-weight properties.[17] In addition, improvements in surface area and electrical conductivity are also highly sought for energy storage materials including hydrogen storage materials and supercapacitors.

This study reveals a new pathway for high-throughput spinning of CNT-reinforced polymer composite fibers and CNT/CF fibers developed through the Forcespinning® (FS) technique. There are several processing methods that exist for the production of NFs such as electrospinning, hydrothermal synthesis, template synthesis, phase separation, self-assembly, shear spinning, and other spinning methods (wet, dry, and melt spinning).[18] Electrospinning has been the preferred method given its potential for industrial production of nanofibers though it presents many limitations such as the need of high electric fields and typically the need of a dielectric solution besides the intrinsic suitable vapor pressure, viscosity, and surface tension to promote optimum fiber formation. Others methods have serious deficiencies when it comes to potential for industrial production and, therefore, have remained attractive for laboratory testing or development of microfibers at the industrial level. Forcespinning® (FS) technology, which was developed by Lozano et al, has the opportunity to offer a high production rate of fine fibers that could range from single digit micron to nanofibers depending on the materials and selected parameters. The absence of electric fields opens up opportunities for low cost fibers with a much broader choice of materials.[18–22] Several systems have been recently produced either from solution or melt, such as polyamide, polyethylene oxide, polylactic acid, polycaprolactone,[22] polypropylene,[23] ultra-high molecular weight polyethylene, (2,5-bis(2′-ethyl-hexyl)-1,4-phenylenevinylene),[19] poly (3′-hexylthiophene (P3HT), Teflon®AF,[24] cellulose, poly(vinylidene fluoride),[21] and indium-tin oxide[25] to mention some. All of the above have produced average fiber diameters in the nano or submicron range. With the use of FS technology, a considerable higher fiber production rate can be obtained. The production rate obtained in this study was 2 g min^{-1}, much higher than the laboratory scale production rate of other techniques such as electrospinning where the production rate is about 0.02 g h^{-1}. The recently developed FS technology utilizes centrifugal force to extrude polymer solutions or melts.[18] Fiber jets are formed by high rotational speeds of a spinneret equipped with nozzles of different diameters. The rotation of the spinneret at high speeds drives the fluid through the orifices. When the centrifugal force and associated hydrostatic pressure exceed capillary forces that tend to restrict the flow of fluid in the orifice, a jet of polymer solution is ejected. Reduction of fiber diameter occurs by the inertial drag between the fiber and the atmosphere as the jet dries.[18–25] The phenomenon of centrifugal force-based spinning is familiar to anyone that has observed cotton candy being made, there are few reports demonstrating its capabilities as a fiber manufacturing technology.

In this study, PAN, a semicrystalline engineering thermoplastic polymer, that is well-known for its applications on ultra-filtration membranes, sails for yachts, and especially as the chemical precursor of fine CFs was used.[2] PAN fibers were developed followed by PAN composite fibers where CNTs were used as the reinforcing phase. The composite fibers were also used as the precursor of CFs. Here, we report a facile and large-scale production method of CFs containing high concentration of well-aligned CNTs. The composite fibers possess enhanced mechanical and electrical properties as well as promising applications for energy storage due to the increased surface area.

EXPERIMENTAL

Materials

Polyacrylonitrile (PAN) (average M_w 150,000), anhydrous *N,N*-dimethylformamide (DMF, 99.9%), sulfuric acid (H_2SO_4, 98%), anhydrous potassium bromide (KBr, >99%), and nitric acid (HNO_3, 70%) were purchased from Sigma–Aldrich. Multiwalled carbon nanotubes (outer diameter 30–50 nm) were purchased from Cheap Tubes Inc. Deionized water (18 MΩ cm) was produced using Mill-Q (Millipore Ltd., UK). The filters used for functionalized CNTs filtration are 0.45 μm filter paper from Millipore. A bath sonicator model cole-parmer 8890 was used. For the spinning of the fiber, a lab scale Cyclone™ L-1000M from Fiberio Technology Corp. was utilized.

Methods

CNTs were functionalized according to Lozano et al. and Ma et al.[26, 27] Briefly, 500 mg of pristine CNTs were added into a 150 mL mixture of acids composed of concentrated sulfuric acid and nitric acid with a volume ratio of 3 : 1. The slurry was sonicated for 4 h at 50°C and refluxed for 12 h at 70°C. The slurry was then diluted with deionized water, and subsequently, it was filtered until a pH of 7 was reached. The CNTs were then dried at 120°C for 24 h.

To prepare the PAN fibers, the procedure consisted of dissolving PAN in DMF at various concentrations and subsequently depositing 2 mL in a cylindrical spinneret. For the CNT-reinforced PAN composite fibers, the functionalized CNTs were dispersed in DMF, and then PAN was added to the suspension, this mixture was then stirred at 80°C for 24 h under an inert atmosphere. The slurry was then injected into the spinneret. The spinning was conducted at various rotating speeds to determine optimal processing parameters for the development of fibers with low diameters, narrow distribution, and absence of beads. The rotational speeds were varied from 3000 to 9000 rpm. At 3000 rpm, the solution was allowed to spin until depletion after 45 s, where at 9000 rpm, it took 10 s. A deep dish fiber collector with equally distanced vertical steel pillars was used to collect the fibers. After collection, the fibers were covered and stored under desiccation.

Figure 1(a) shows the schematics of the fiber formation process. The polymer solution is forced by centrifugal force through the orifices of the spinneret and the web is collected on the designed collector system. Figure 1(b) shows the photograph of the spun PAN and CNT/PAN nonwoven fiber mats. The inserted image in Figure 1(b) shows the spun CNT/PAN composite fiber mats at varying CNTs concentrations.

The carbonization of the nonwoven composite fiber mat was performed in a tubular quartz reactor. First, oxidative stabilization of the fiber was completed at 230°C in air for 6 h. Then, the samples were heated up to 900°C at a heating rate of 2°C

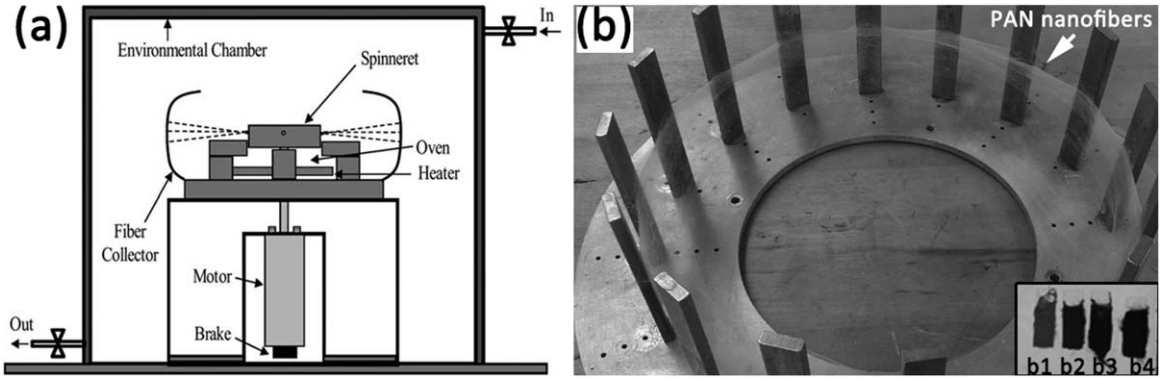

Figure 1. (a) Schematic of Forcespinning® setup. (b) Photograph of spun PAN fibers web (cycle time 30 s, arrow labeled) in lab scale system. Figure 1b inserted images, spun CNT/PAN composite fibers at various CNTs concentrations: b1, 5% CNTs, b2, 8% CNTs, b3, 10% CNTs, b4, 15% CNTs.

min^{-1} in an atmosphere of Ar and kept at 900°C for 2 h before cooling down to room temperature.

Characterization

The morphology of the collected fibers was evaluated using a scanning electron microscope (SEM, Sigma VP, Carl Zeiss, Germany). Thermogravimetric analysis (TGA), differential scanning calorimetry (DSC), and Dynamic mechanical analysis (DMA) were performed using TA-Q series equipments, TGAQ500, DSCQ100, and DMAQ800, respectively. Samples used for TGA and DSC examination were about 10 mg, and scans were performed at a rate of 10°C min^{-1}. Raman measurement was performed using a Bruker Senterra Raman spectrometer with a 785 nm excitation laser. Fourier transform infrared spectroscopy (FTIR) was performed with Bruker IFS 55 Equinox FTIR spectrophotometer using KBr pellets. Electrical conductivity was analyzed using a four point probe tester JANDEL RM2 (Jandel Engineering, Ltd., USA). The BET (Brunauer–Emmett–Teller) surface area of the samples was measured by N_2 adsorption using a Micromeritics ASAP 2020 surface area analyzer.

RESULTS AND DISCUSSION

This work represents the first report of development of PAN fibers and CNT-reinforced PAN composite fibers by utilizing centrifugal forces. Figure 2(a) shows SEM images of developed PAN fibers (inserted image show the photograph of the spun PAN fibers) whereas Figure 2(b) displays the diameter distribution. The fiber diameter distribution appears to follow a log-normal function; this sample exhibits an average log(diameter, micrometers) of −0.2 (630 nm) with a standard deviation of 0.10 (500–800 nm). To ensure reproducibility of the results, two batches of fibers were made independently for each condition, and both low and high magnification images were analyzed. The average fiber diameter and other data related to fiber dimensions are based on the average of all measurements that were made (more than a few hundred per sample with random image sampling).

The fiber morphology and diameter are influenced by several variables including spinneret configuration, spinneret temperature, and collector distance, but the main factors are the concentration of the polymer solution and the spinneret rotational speed (rpm). Our systematic investigations revealed that the concentration had a stronger effect on fiber characteristics compared to other factors [Figure 3(a–d)]. Beads can be found in samples with a PAN concentration of 11 wt %, and this effect can be related to the lower value of viscosity against surface tension. Increasing the PAN concentration from 11 to 14 wt % led

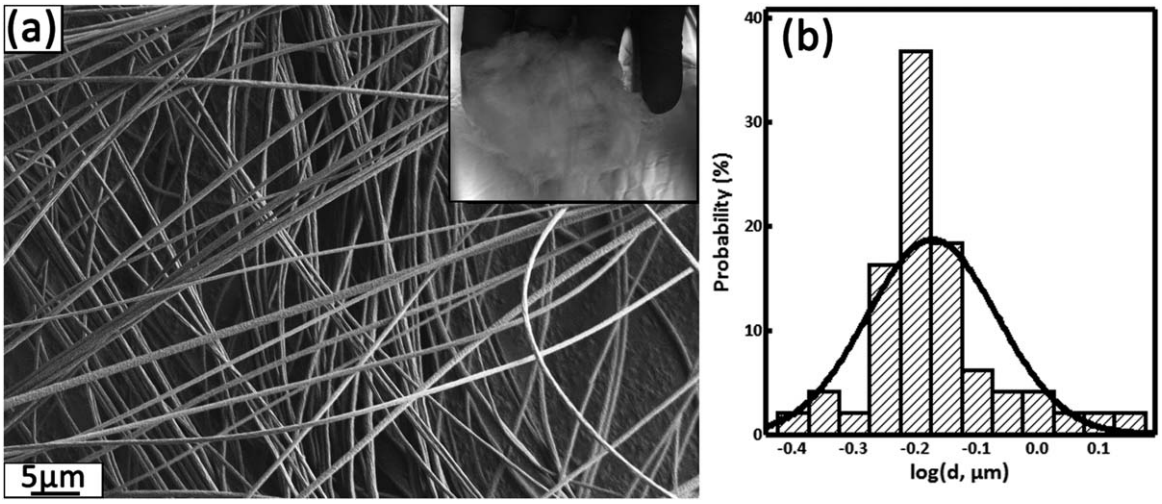

Figure 2. (a) Typical SEM image of spun PAN fibers, (inserted images, photograph of the spun fibers). (b) Diameter distribution of spun PAN fibers.

to a significant decrease in bead formation though fiber diameter was increased from 400 nm (log$d$, −0.39) to 1.2 μm (log$d$, 0.08) [Figure 3(e)]. Dynamic shear experiments [Figure 3(f)] revealed nearly an order of magnitude reduction in shear viscosity of the PAN solution, from 1.33 Pa s at 15% to 0.22 Pa s at 11% at 50 Hz. Therefore, the thinner fibers obtained at lower concentrations are due to low viscosity and additional stretching before solvent evaporation. Although, at concentrations lower than 12%, the beading morphology cannot be avoided. As previously reported, when the solutions have low viscosity and poor elastic contribution the fibers tend to break preventing the formation of uniform fibers, and as a result, droplets or necklace-like structures known as "beads-on-string" are formed. With increasing viscosity, the viscoelastic jet tends to take longer time to break up or does not break up at all, and if extensional deformation due to centrifugal forces is fast compared to the inverse of the fluid relaxation time beadless continuous long fibers is formed.

Spinneret rotational speed has a more subtle effect on fiber formation (Figure 4). At a speed of 3,000 rpm, the fibers were 630 nm in diameter. Increasing the speed to 9,000 rpm resulted in less output of fibers, while average fiber diameter slightly increased to 700 nm. Higher spinneret speeds produced fibers with narrower diameter distribution due to the decrease of thick fibers given the higher centrifugal force. The FS system does not require a positive displacement feed system to deliver the solution through the orifice. The polymer mass flow rate through the spinneret is actually partially governed by pressure driven flow from the outward centrifugal force acting on the solution at the spinneret entrance. Therefore, higher flow rates can overcome the decrease in yield observed at higher angular velocities. Although this study has revealed some very important capabilities of this process, a more thorough systematic investigation is forthcoming regarding the relations of the shear rate, fluid elasticity, and aerodynamic analysis in defining fiber formation.

To obtain PAN fibers with high concentration of CNTs, the CNTs solution has to be prepared with high concentration. There are mostly three methods that have been successfully used to disperse CNTs into solvents and polymer matrices: (1) physical blending, (2) chemical functionalization, and (3) dispersants-assisted dispersion. For physical blending, mechanical forces such as sonication are used, although simple and cost effective, the quality of the dispersion is often the poorest. The so-dispersed nanotubes will quickly precipitate as sonication stops. Another method relies on the use of a surfactant. The surfactant can attach to the surface of the CNTs to disentangle the bundles while sonicated. Other chemical routes involve the use of additives to alter the surface tension of the CNTs to prevent surface tension-driven defects while mixing with polymers though the presence of additives has been reported to alter the conductivity and mechanical properties of the system. Another route is to functionalize the CNTs to be water or organic

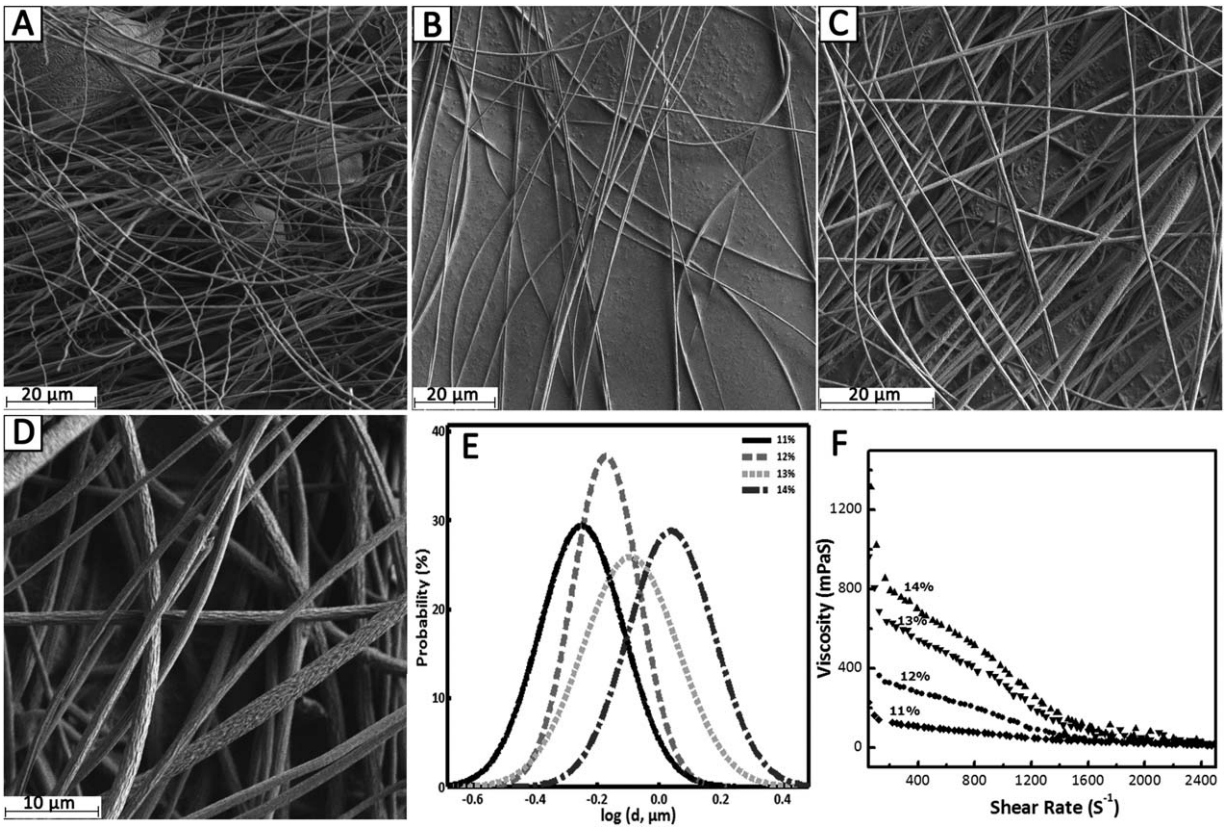

Figure 3. SEM images of spun PAN fiber with PAN concentrations of 11% (a), 12% (b), 13% (c), and 14% (d), respectively. (e) Diameter distributions of PAN fibers at various PAN concentrations (log$d$ = −0.39, −0.2, −0.11, and 0.08, respectively, for 11%, 12%, 13%, and 14% PAN fibers, respectively). (f) Shear viscosity as a function of shear rate of polymer solutions at various concentrations.

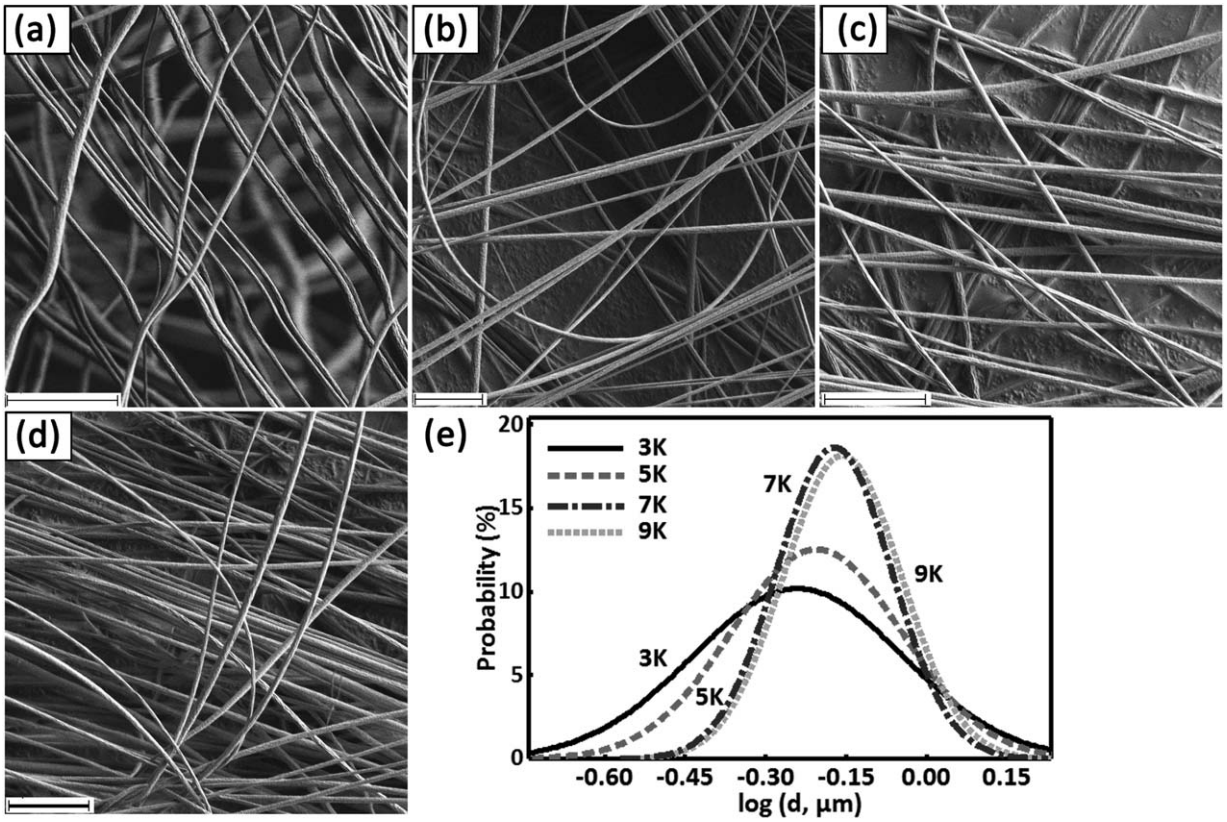

Figure 4. SEM images of spun 12% PAN at the rotating speeds of 3000 (a), 5000 (b), 7000 (c), and 9000 (d). (e) Diameter distribution of spun 12% PAN DMF solution at various rotating speeds. The length of the bar is 1 μm.

solvent soluble. The CNTs are treated with strong oxidizing reagents such as strong mineral acids to form carboxylic acid groups or hydroxyl groups on the nanotube walls. To solve the problem of aggregation, and also to increase the affinity to the desired polymer, in this case PAN, the CNTs were functionalized with 3 : 1 (*V:V*) H_2SO_4 and HNO_3 at 70°C to generate carboxylic acid groups. After functionalization, the CNTs can be well dispersed in water, and organic solvents such as DMF and chloroform without precipitation for several months.

From the inserts in Figure 1(b), it can be observed that the concentration of CNTs in the PAN fibers significantly alters the color of the composite. SEM images (Figure 5) show that the surface morphology of the composite fibers is rougher compared to pure PAN fibers. CNTs are observed to be wetted by the PAN [cross section images, Figure 5(e,f)]. The CNT are well embedded into the matrix of the PAN polymer. With the increase in the concentration of CNTs in PAN, the fiber diameter increases due to the increase of viscosity after CNTs addition.

Figure 6 shows TGA [Figure 6(a–d)] and DSC graphs [Figure 6(e,f)] of PAN and the CNTs-reinforced PAN composite fibers under nitrogen and oxygen at a heating rate of 10°C min^{-1}. The DSC curve of PAN fibers [Figure 6(e)] shows a degradation peak at 295°C, whereas the composite fibers [Figure 6(f)] have a degradation peak at 311°C, the increased thermal stability indicates the existence of a CNT/PAN interface. In the TGA curve, it should be noted that the difference in weight percentage at degradation corresponds to the content of CNTs in the composite fiber which is around 15 wt %.

The composite fibers were burned at 450°C (higher temperature than PAN degradation though lower than CNTs degradation) for 2 h in oxygen to further identify the status of CNTs in the composite fibers. Figure 7 shows SEM images of 400 and 450°C (2 h) post-treated PAN/15 wt % CNT composite fibers. It can be observed that the CNTs are well aligned along the axis of the spun fiber. In the CNT/PAN composite, the polymer wraps the aligned CNTs, For 450°C post-treated sample, a continuous CNTs network is observed. In most reported solutions such as chloroform, DMF and other organic solvents, the dispersed behavior of CNTs in the solution is isotropic, except in chlorosulfonic acid solutions, where the CNT form anisotropic nematic liquid crystal phases.[28] Here, the CNTs are randomly oriented in the polymer solution, so spinning it into a fiber form is crucial for alignment.[18–22]

Figure 8 compares the SEM images of the PAN and CNT/PAN composite fibers after carbonization. As indicated, the carbonized composite fibers are rougher compared to the CNT/PAN composite. CNTs can be observed embedded in the fibers from the cross-section view [Figure 8(e,d,f)]. The increased surface roughness in the ultimate CNT/CF fiber system positively impacts the properties derived from surface area enhancements. Table I summarizes the BET surface area, the pore volume, mesopore volume, and average pore size for the carbonized fibers. The surface properties of CNTs are also listed in Table I for

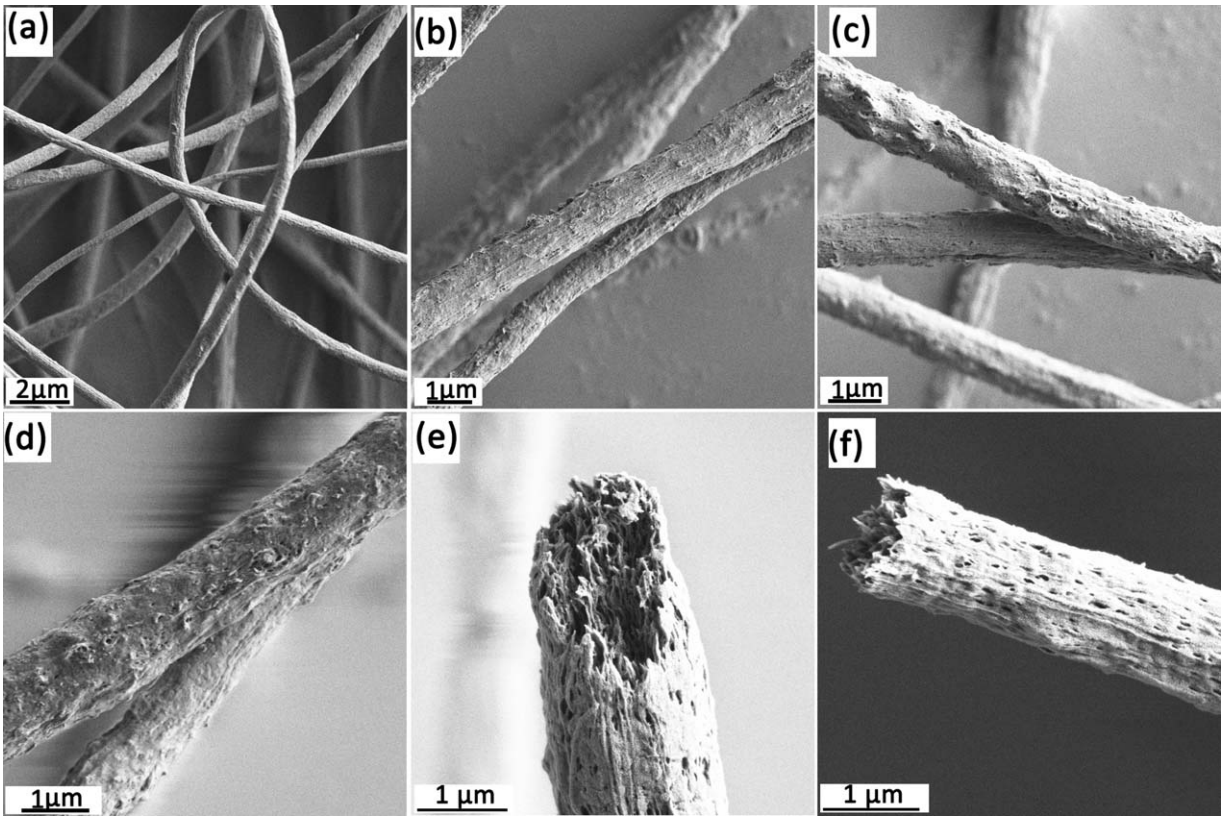

Figure 5. SEM images of PAN/CNTs fiber composites at CNTs contents of 3% (a), 8% (b), 10% (c), 15% (d–f). Figure (e) and (f) are the images of the cross sections of fibers (d).

comparison with the fibers. The mesopore and micropore volumes of the CNT/CFs are higher than that of the CFs. In addition, the electrical conductivity of the CFs is also improved after the addition of CNTs. Based on the increased porosity and electrical conductivity, the CNT/CFs fibers possess promising applications in energy storage areas.

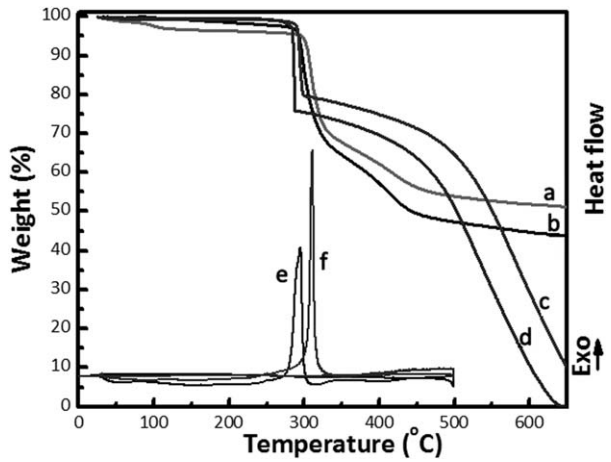

Figure 6. TGA curves (a–d) of PAN and CNT/PAN fibers with 15% of CNT concentration in oxygen (c: PAN/CNTs, d: PAN) and nitrogen (a: PAN/CNTs, b: PAN) atmospheres, and DSC curves (e and f) of PAN (e) and PAN/15% CNTs fibers (f).

Raman spectrum [Figure 9(a)] of multiwalled CNTs indicates three characteristic peaks. The *G*-line peak at 1580 cm^{-1} corresponds to the high-frequency Raman-active E_{2g} mode of graphite, the *D*-line at 1320 cm^{-1} is attributed to disorder-induced carbon features arising from finite particle size effect or lattice distortion,[29] and another peak located at 850 cm^{-1} which is assigned to the C═O stretching vibrational peak. In the CNT/PAN composite, the peak positions of the CNTs are not changed, suggesting that the lattice structure of the CNTs were not significantly affected by the presence of the PAN. After the carbonization, the relative intensity of *G*-line becomes weaker, indicating that the intrinsic electronic properties (symmetry of the bonds) of the hexagonal carbon skeleton were affected. Based on these observations, we can speculate that there are π–π stacking interactions between the hexagonal carbon networks of carbonized PAN fibers with the hexagonal carbon networks of CNTs, resulting in the changes of the vibrational asymmetry of the carbon skeleton.

Figure 9(b) compares the FTIR spectra for (a) carboxylic functionalized CNTs, (b) pristine PAN fibers, and CNT/PAN composite fibers. As indicated, the intrinsic peak of multiwalled CNTs is at 1631 cm^{-1}, assigned to the C═C stretching vibration mode associated with sidewalls of the CNTs. After the acid treatment, an additional peak was observed at 1713 cm^{-1}, which corresponds to the carboxyl group stretches (C═O). The broad band at 3440 cm^{-1} is attributed to —OH stretching in carboxylic acid group. PAN also has a strong peak at

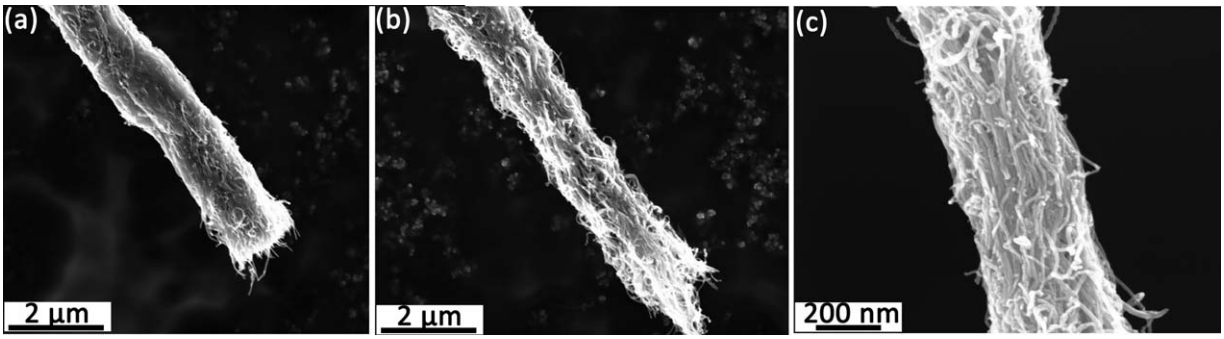

Figure 7. SEM images of 400°C (a) and 450°C (b) post-treated PAN/15%CNTs composite fibers. (c) is the magnified images of 7b.

2244 cm^{-1}, assigned to the nitrile group of PAN. The strong polar bond of —CN has stronger signals in FTIR than in Raman. After the addition of the CNTs into the PAN matrix, the nitrile peaks of the PAN and functionalized CNTs all decreased, and the intensity of the C=C stretching vibration increased slightly, due to the increase content of CNTs in the matrix. After carbonization, both the nitrile peak and the methyl peak (at 2943 cm^{-1}) disappeared. Though the peak at 1631cm^{-1} was enhanced, which corresponds to the C=C stretching vibration mode associated with sidewalls of the CNTs. FTIR results confirm the observation of Raman spectroscopy results, the electric polarity of the sidewalls of the CNTs has changed, resulting from the covalent π–π stacking interactions between the hexagonal carbon networks of carbonized PAN fibers with the hexagonal carbon networks of CNTs.

The carbonized PAN fibers have an electrical conductivity of 0.16 S cm^{-1}. The carbon material prepared at relatively low temperature is disordered, containing partly sp^3 carbon and substantial dangling oxidation bonds, as Raman and FTIR indicated (peaks around 1073 cm^{-1}, Figure 9). The conductivity of the carbonized fibers is affected by the level of the band gap generated by the defects. The electrical conductivity of the carbonized CNT/PAN fibers was tested to be 10.62 S cm^{-1}, which is 100-fold greater than that of carbonized PAN fibers, as tabulated in Table I.

Typical stress–strain curves of CNT/CFs composite fiber mats are shown in Figure 10. CNTs improved the tensile strength of the composite fiber mat. The tensile strength showed a peak value of 10 MPa at about 15% CNTs with a 250 % improvement. According to Curran et al. suggestion,[30] for a simple composite system without micromechanical interlocking and chemical bonding between the filler and matrix, the load transfer from a matrix to filler is provided through weak Van der Waals bonds between the filler and the matrix. Given the calcinations procedure where as shown by FTIR and Raman analysis where interactions between the matrix and the CNTs were observed, the tensile strength of the composite fibers was expected to increases with increasing CNTs content. The strain

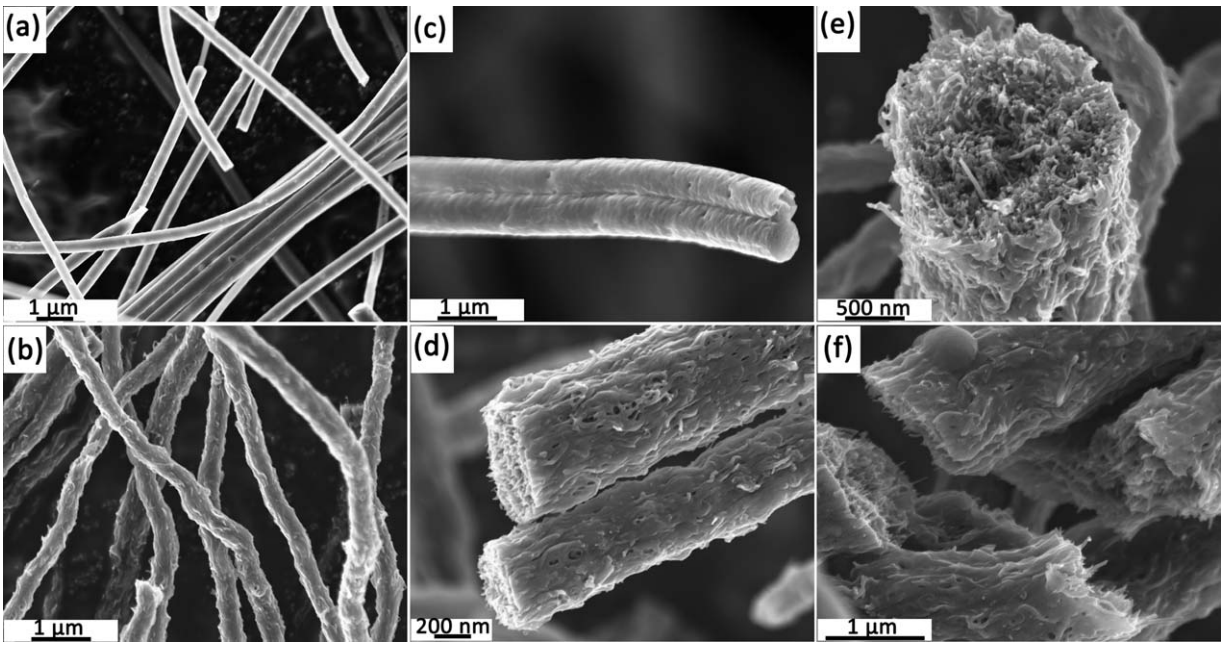

Figure 8. SEM images of carbonized PAN fibers (a), and carbonized PAN/15%CNTs composite fibers (b). (c) is the cross section image of (a), and (d)–(f) are the cross section images of (b).

Table I. Surface Properties and Electrical Conductivity of Carbonized Fibers

Sample	S_{BET} (m^2 g^{-1})	V_{total} (cm^3 g^{-1})	V_{mic}(cm^3 g^{-1})	V_{mes}(cm^3 g^{-1})	P_D (nm)	σ (S cm^{-1})
CNTs	128	0.139	0.017	0.122	2.63	
Carbonized Fiber	154	0.167	0.021	0.146	0.40	0.16
15 %CNTs in CFs	790	0.286	0.105	0.182	1.91	10.62

S_{BET}, specific surface area; V_{total}, total pore volume; V_{mic}, micropore volume; V_{mes}, Mesopore volume; P_D, pore size

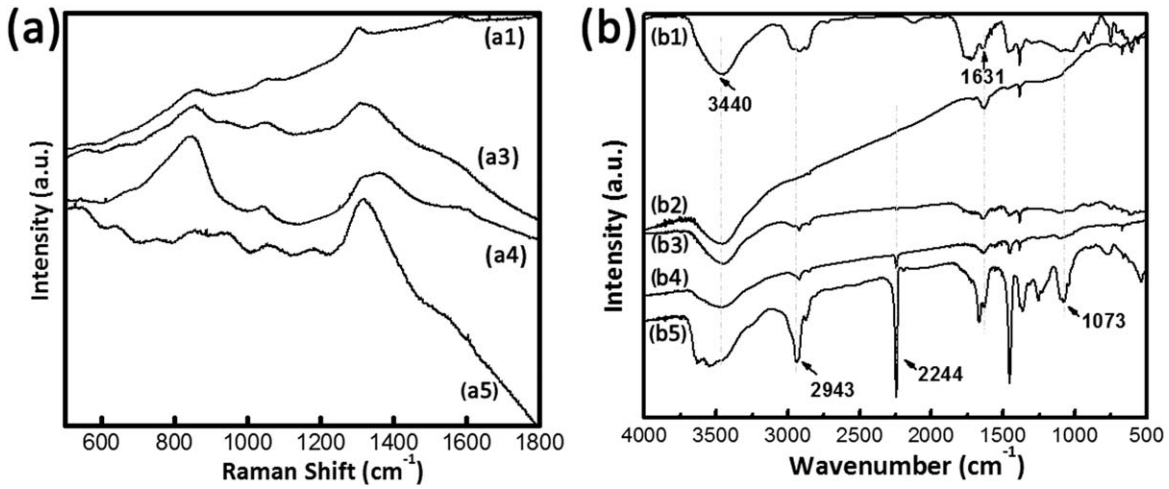

Figure 9. Raman (a) and FTIR (b) spectra of CNTs (a1, b1), PAN (b2), 3% CNTs/PAN (a3, b3), 15% CNTs/PAN (a4, b4) and carbonized 15% CNTs/PAN fiber (a5, b5). The dash lines are added in the FTIR spectra for better observations.

to break decreased with the increase of the CNTs in the composite fibers. Improvements on tensile strength in most of the reported CNT/polymer composites are coupled with a reduction in strain at break.[31]

In this study, the carbonization process did not follow with a graphitization process to further increase mechanical properties since the main goal was to develop optimal processing parameters to develop fibers with high concentration of CNTs at a large-scale. These composite fibers show improved mechanical and electrical properties especially after following the one-step carbonization method.

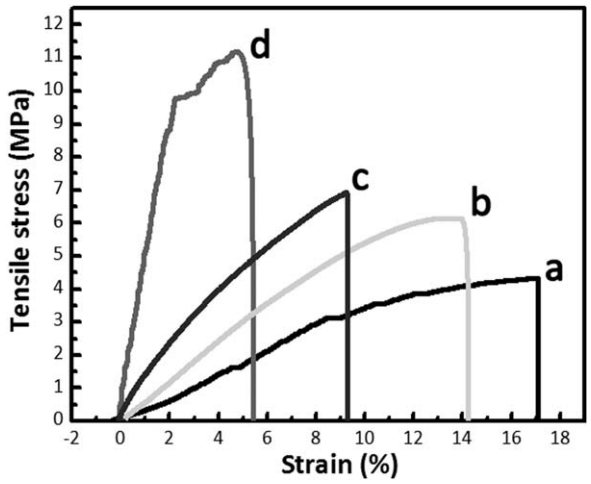

Figure 10. Truly tensile strength curves of carbonized PAN (a), and carbonized PAN/CNTs fibers with 3% CNTs (b), 8% CNTs (c), and 15% CNTs (d).

CONCLUSIONS

A facile and large-scale method for the production of PAN fibers, CNT-reinforced composites CFs, and CNT-reinforced PAN composite fibers was developed. CNTs were well aligned along the axes of the fibers and formed a continuous network embedded within the matrix. Raman and FTIR spectra suggest interactions between CNTs and the carbonized PAN fibers through π–π stacking interactions. The CNTs network, embedded into the polymer matrix has different thermal shrinking properties from that of PAN. Compared to pristine CFs, the CNT-reinforced fibers show improved electrical properties and higher tensile strength.

ACKNOWLEDGMENT

This work was financially supported by Fiberio Technology Corporation.

REFERENCES

1. Bacon, R. *J. Appl. Phys.* **1960**, *31*, 283.
2. Chawla, S.; Naraghi, M.; Davoudi, A. *Nanotechnology* **2013**, *24*, 255708.

3. Othman, R. N.; Kinloch, I. A.; Wilkinson, A. N. *Carbon* **2013**, *60*, 461.
4. Iijima, S. *Nature* **1991**, *354*, 56.
5. Zhang, G.; Dang, L.; Li, L.; Wang, R.; Fu, H.; Shi, K. *CrystEngComm* **2013**, *15*, 4730.
6. Prasad, S. K.; Kumar, M. V.; Yelamaggad, C. V. *Carbon* **2013**, *59*, 512.
7. Wang, J.; Xu, H.; Yang, D.; Wu, Y. *Fiber. Polym.* **2013**, *14*, 571.
8. Othman, R. N.; Kinloch, I. A.; Wilkinson, A. N. *Carbon* **2013**, *60*, 461.
9. Kroustalli, A.; Zisimopoulou, A. E.; Koch, S.; Rongen, L.; Deligianni, D.; Diamantouros, S.; Athanassiou, G.; Kokozidou, M.; Mavrilas, D.; Jockenhoevel, S. *J. Mater Sci-Mater M.*, **2013**, *24*, 2889.
10. Lal, M.; Singhal, S. K.; Sharma, I.; Mathur, R. B. *Appl. Nanosci.* **2013**, *3*, 29.
11. Dubal, D. P.; Holze, R. *New J. Chem.* **2013**, *37*, 403.
12. Qian, M.; Goh, C. S.; Sun, Y. H.; Ng, F. L. *Compos. Part A-Appl. Sci. Manuf.* **2013**, *48*, 67.
13. Thostenson, E. T.; Karandikar, P. G.; Chou, T. W. *J. Phys. D-Appl. Phys.* **2005**, *38*, 3962.
14. Li, S.; Sun, B.; Imai, H.; Mimoto, T.; Kondoh, K. *Compos. Part A-Appl. Sci. Manuf.* **2013**, *48*, 57.
15. Dror, Y.; Salalha, W.; Khalfin, R. L.; Cohen, Y.; Yarin, A. L.; Zussman, E. *Langmuir* **2003**, *19*, 7012.
16. Li, W. J.; Laurencin, C. T.; Caterson, E. J.; Tuan, R. S.; Ko, F. K. *J. Biomed. Mater. Res.* **2002**, *60*, 613.
17. Li, Y.; Shen, M.; Su, H.; Chiang, C.; Yip, M. *J. Nanomater* **2012**, *2012*, Article ID 262694, 6 p.
18. Sarkar, K.; Gomez, C.; Zambrano, S.; Ramirez, M.; Hoyos, E.; Vasquez, H.; Lozano, K. *Mater. Today* **2010**, *13*, 12.
19. Padron, S.; Patlan, R.; Gutierrez, J.; Santos, N.; Eubanks, T.; Lozano, K. *J. Appl. Polym. Sci.* **2012**, *125*, 3610.
20. Padron, S.; Fuentes, A.; Lozano, K. *J. Appl. Phys.* **2013**, *113*, 024318.
21. Vazquez, B.; Vasquez, H.; Lozano, K. *Polym. Eng. Sci.* **2012**, *52*, 2260.
22. McEachin, Z.; Lozano K. *J. Appl. Polym. Sci.* **2012**, *126*, 473.
23. Raghavan, B.; Soto, H.; Lozano, K. *J. Engin. Fiber.Fabr.* **2013**, *8*, 52.
24. Rane, Y.; Altecor, A.; Bell, N. S.; Lozano, K. *J. Eng. Fiber. Fabr.* **2013**, *8*, 88.
25. Altecor, A.; Mao, Y. B.; Lozano, K. *Funct. Mater. Lett.* **2012**, *5*, 1250020.
26. Lozano, K.; Files, B.; Rodriguez-Macias, F.; Barrera, E. V. *Powder Mater-Current Rese. Indust. Pract.* **1999**, 333.
27. Ma, P.; Siddiqui, N. A.; Marom, G.; Kim, J. K. *Compos. Part A-Appl. Sci. Manuf.* **2010**, *41*, 1345.
28. Davis, V. A.; Parra-Vasquez, A. N. G.; Green, M. J.; Rai, P. K.; Behabtu, N.; Prieto, V.; Booker, R. D.; Schmidt, J.; Kesselman, E.; Zhou, W.; Fan, H.; Adams, W. W.; Hauge, R. H.; Fischer, J. E.; Cohen, Y.; Talmon, Y.; Smalley, R. E.; Pasquali, M. *Nat. Nanotech.* **2009**, *4*, 830.
29. Hadjiev, V. G.; lliev, M. N.; Arepalli, S.; Nikolaev, P.; Files, B. S. *Appl. Phys. Lett.* **2001**, *78*, 3193.
30. Curran, S. A.; Ajayan, P. M.; Blau, W. J.; Carroll, D. L.; Coleman, J. N.; Dalton, A. B. *Adv. Mater.* **1998**, *10*, 1091.
31. Moniruzzaman, M.; Chattopadhyay, J.; Billups, W. E.; Winey, K. I. *Nano Lett.* **2007**, *7*, 1178.